



Power Electronic Systems
Laboratory

© 2017 IEEE

Proceedings of the IEEE International Electric Machines & Drives Conference (IEMDC 2017), Miami, FL, USA, May 21-24, 2017

A High Torque, Wide Air Gap Bearingless Motor with Permanent Magnet Free Rotor

T. Holenstein,
J. Greiner,
D. Steinert,
J. W. Kolar

This material is published in order to provide access to research results of the Power Electronic Systems Laboratory / D-ITET / ETH Zurich. Internal or personal use of this material is permitted. However, permission to reprint/republish this material for advertising or promotional purposes or for creating new collective works for resale or redistribution must be obtained from the copyright holder. By choosing to view this document, you agree to all provisions of the copyright laws protecting it.



Eidgenössische Technische Hochschule Zürich
Swiss Federal Institute of Technology Zurich

A High Torque, Wide Air Gap Bearingless Motor with Permanent Magnet Free Rotor

Thomas Holenstein¹, Jonas Greiner¹, Daniel Steinert², Johann W. Kolar¹

¹Power Electronic Systems Laboratory, ETH Zurich, Zurich, Switzerland

²Levitronix GmbH, Zurich, Switzerland

Abstract—This paper introduces a bearingless motor topology with a magnet free rotor, which enables higher rotor torque densities and wider air gap compared to previously published topologies. Flux density in the air gap and therefore torque capability is maximized by a stator in temple configuration, which provides large winding space. The low number of eight stator and six rotor teeth keeps stray flux low, which enables wider air gap ratios at the same time. A challenge of having a low teeth number are large angle dependent force and torque nonlinearities, which are compensated in the control algorithm. A 3D FEM optimized prototype was constructed and put into operation. Measurements of the running system are presented to confirm the feasibility of the introduced topology.

Keywords—*temple motor, magnetic levitation, reluctance rotor, high torque, wide air gap machine.*

I. INTRODUCTION

Research on bearingless motors has been popular for many years. Especially the bearingless slice motor offers very unique advantages, which have led to several commercial products [1]. The advantages are mostly connected to the fact, that the rotor can be completely separated and isolated from the stator in a very simple manner. This allows to rotate the rotor contactless in its own containment in the widest range of environmental conditions, without the need for a special stator. The thereby achieved simplicity can lead to cost effective drive systems for special applications, where the added hardware and software complexity compared to conventional drive systems is outweighed. Examples are ultra-pure, low shear fluid handling, harsh environmental conditions like aggressive chemicals, abrasive media, extreme ambient temperatures or single-use applications. The use of a bearingless slice motor as pump, blower or mixer for such applications was first mentioned in [2].

Several new topologies without permanent magnets in the rotor have been published recently [3]. These topologies feature either a low mechanical complexity [4], a wide air gap to rotor radius ratio [5], further called gap factor G , or a good torque per stator permanent magnet mass ratio [6]. In theory, reluctance rotors have advantages for very high temperatures, where permanent magnets would demagnetize, for very high speeds due to higher material strength and also for disposable applications due to lower manufacturing cost of the rotor. However, due to very low achievable torque, or small realizable air gap ratios these topologies need a relatively large rotor with less air gap to achieve the same performance as a comparable permanent magnet rotor topology [7], [8], [9]. This

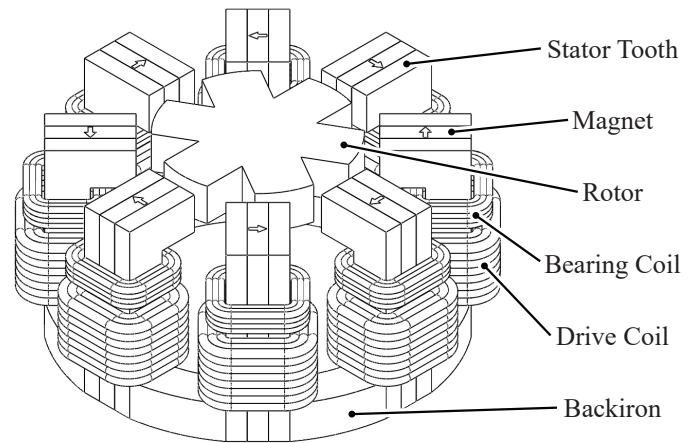


Fig. 1: Introduced motor topology in temple configuration with eight stator teeth, a six teeth reluctance rotor and separated bearing and drive windings.

in turn leads to worse thermal insulation between rotor and stator, higher circumferential speeds and higher manufacturing cost of the rotor, whereby most of the theoretical advantages may be nullified.

To overcome these limitations, a new bearingless motor topology in temple configuration is presented in this work (see Fig. 1). For the targeted applications, maximum performance per rotor volume is needed, with motor outer dimensions being uncritical. The stator configuration, which reaches around and below the rotor, gives room for a very large winding space, such that the air gap flux density and therefore the torque can be maximized. Unlike the conventional temple motor design [10], where the stator is iron and the rotor a permanent magnet, our design has flux-switching like stator teeth containing permanent magnets which are magnetized tangentially in alternating direction. Most research on flux-switching permanent magnet motors is done on small air gaps and large stator and rotor teeth numbers with 12/10 being the smallest popular combination [11], [12]. We will do the opposite and choose the low number of eight stator and six rotor teeth. This keeps stray flux low and enables a larger air gap to rotor radius ratio, at the cost of a nonlinear angle dependent bearing force generation. Fig. 2 shows the evolution from a conventional temple motor with a PM rotor to the presented topology with reluctance rotor and stator permanent magnets.

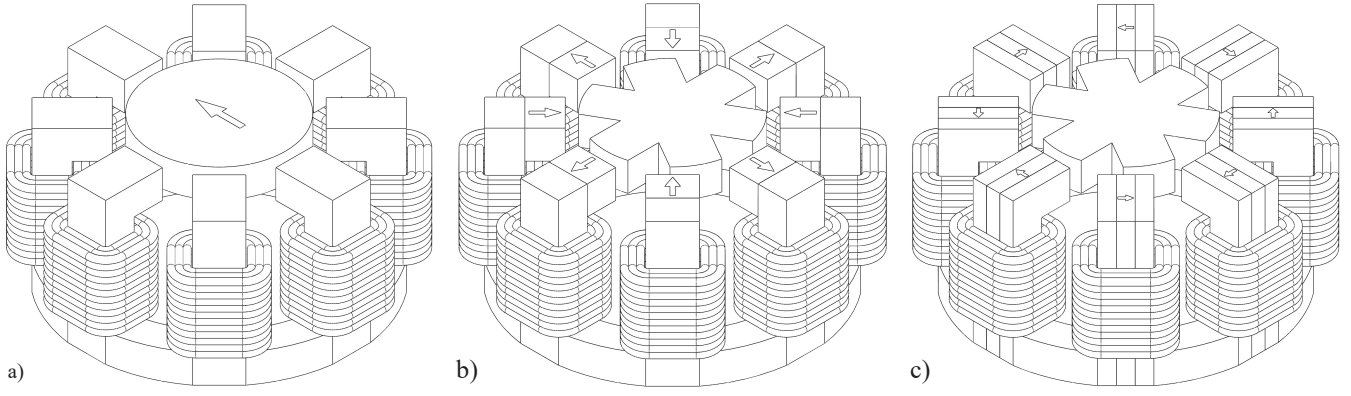


Fig. 2: Temple motor topologies: a) conventional motor with permanent magnet rotor, b) permanent magnet biased reluctance motor, c) flux-switching temple motor.

II. MOTOR DESIGN

A prototype system of the new topology was designed. The used 3D FEM Model can be described by roughly twelve parameters that are shown in Fig. 3. The following boundary conditions were given in advance:

- Rotor outer radius $r_{o,r}$.
- Stator inner radius $r_{i,s}$.
- Limitation of permanent magnet mass in the stator.
- Current limitation through ohmic loss limitation.

This leaves the following ten parameters to be optimized:

- Rotor inner radius $r_{i,r}$.
- Rotor middle radius $r_{m,r}$.
- Rotor tooth width $w_{tooth,r}$.
- Rotor height h_{rotor} .
- Stator tooth width $w_{tooth,s}$.
- Stator magnet width w_{mag} .
- Stator middle radius $r_{m,s}$.
- Stator outer radius $r_{o,s}$.
- Motor height h_{motor} .
- Back iron height $h_{backiron}$.

A multi-objective optimization procedure with the following objectives was used:

- Maximization of torque output.
- Maximization of passive axial and tilting stiffness values.
- Maximization of active bearing force to passive radial stiffness ratio.
- Minimization of cogging torque.
- Minimization of angle dependent bearing force and torque fluctuation.

Due to the complex nature of this optimization problem and the significant runtime of 3D FEM simulations an iterative manual approach based on knowledge from previous bearingless motor topologies was used to find a converging solution with a minimum amount of required simulations. The simulated performance values, averaged over one rotation, of the finally chosen geometry are summarized in Table I. With a gap factor $G = 10\%$, which resulted from the boundary conditions, a rotor torque density $\tau = \frac{T}{V_{rotor}} = 45 \text{ Nm/l}$

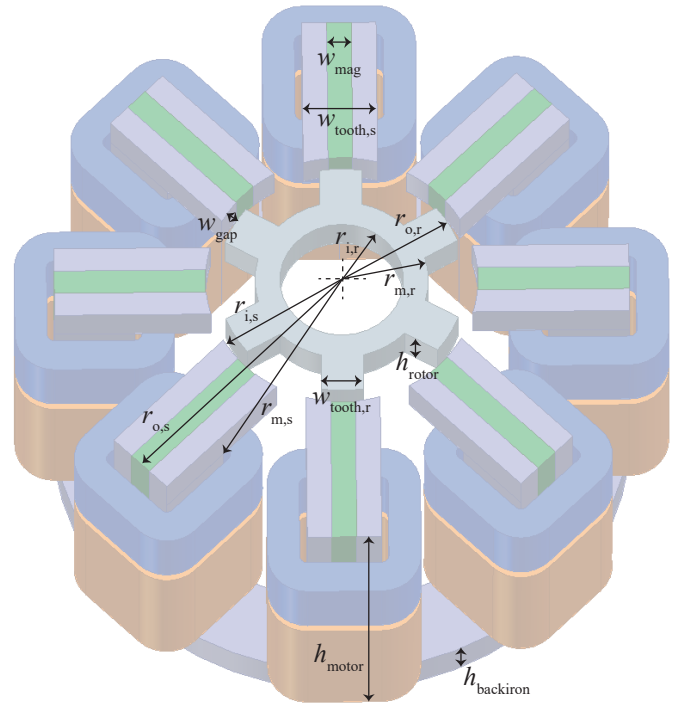


Fig. 3: FEM simulation model used to find the optimal geometry. All dimensions that were optimized or given from the boundary conditions are shown.

could be reached. These values are significantly higher than for existing bearingless slice motor topologies with reluctance rotor. For example in [6] with $G = 4\%$, $\tau = 11 \text{ Nm/l}$ was reached.

III. OPERATING PRINCIPLE

A characteristic of bearingless slice motors is, that apart from rotation only two radial degrees of freedom need to be actively stabilized, which is most commonly realized with just one additional three phase system. Tilting motion in two degrees as well as axial movement are passively stable through reluctance forces. An applied force will however lead to a

TABLE I: Simulated Electromechanical Properties of the Prototype

Parameter	Value	
Passive Properties		
Radial stiffness	k_r	130 N/mm
Axial stiffness	k_z	14.7 N/mm
Tilting stiffness weak axis	k_{α}	0.28 Nm/deg
Tilting stiffness strong axis	k_{β}	0.42 Nm/deg
Active Properties		
Torque @ 250W ohmic losses	T_{max}	9.1 Nm
Torque constant	k_T	6 mNm/At
Radial bearing force constant	k_F	0.13 N/At

deflection in the passive degrees of freedom, and might excite oscillations which are only slowly damped. Rotor loads need to be carefully designed in terms of maximum load, center of gravity and unbalance.

The operation principle of FSPM motors is very similar to rotor PM machines due to the sinusoidal back-EMF. To generate torque, an air gap field with the number of rotor poles p has to be generated by the stator coils. Radial force is generated with a $p \pm 2$ field. Slice motors are realized with concentrated windings, since ohmic losses in the winding head would be dominant for distributed windings. Both combined and separated winding systems can be used to generate an air gap field for torque and radial force generation. For our prototype, in order to be able to use an existing six phase power electronics converter, separated bearing and drive coils are used. An eight phase power electronics would be needed for combined windings on our prototype.

To generate the required air gap field, the phase shift between adjacent stator coils for our FSPM 8/6 topology should be 90 degrees for torque generation and 45 degrees for force generation. This would be realizable with a two-phase drive winding and a four-phase bearing winding. For simplicity, we do however also use a two-phase bearing winding, which results in an average angle deviation of 22.5 degrees, respectively a distribution factor of 0.924, and therefore a small decrease of maximum achievable bearing force. This is shown in Fig. 4.

Since we now have a two-phase drive and two-phase bearing motor, we are able to connect it to an existing bearingless motor controller with six IGBT half-bridges and four current sensors, which is normally used for motors with two three phase systems. The two half bridges with current sensors are connected to phase A and B of the drive respectively bearing coils, whereas the third half bridge is used as return path for both phases and normally switched at 50% duty-cycle. Fig. 5 shows the connection scheme of the sixteen motor coils to the six power phases of the prototype.

IV. CONTROL DESIGN

The control design of the introduced topology was quite challenging. Compared to rotor PM motors several new aspects were observed and had to be considered to successfully levitate the rotor:

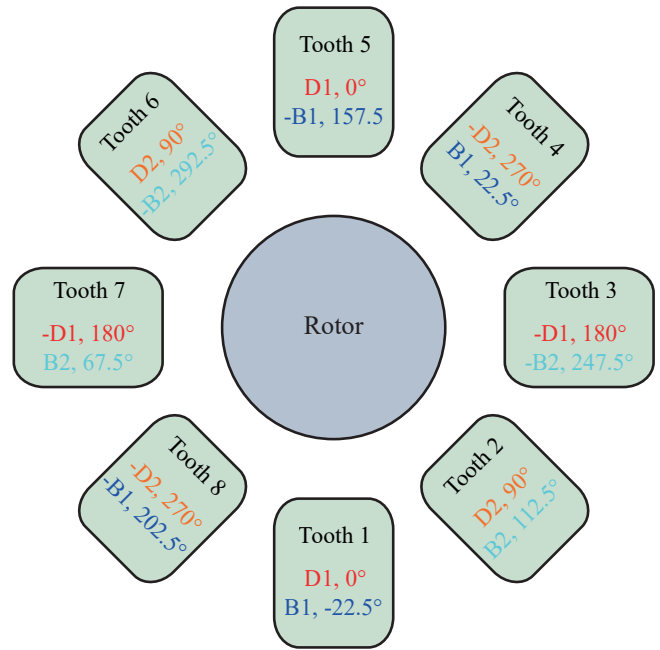


Fig. 4: Winding scheme. Shown are drive phases D1 (0 deg), D2 (90 deg) and bearing phases B1 (0 deg) and B2 (90 deg).

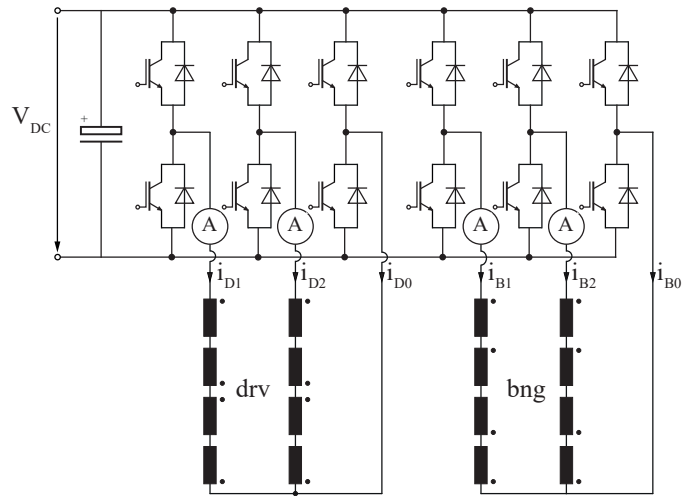


Fig. 5: Connection scheme of drive coils (drv) and bearing coils (bng) to the six phase bearingless motor controller.

- Angle dependent variation of radial force constant k_F by a factor of three.
- Angle dependent coupling between radial x and y force component.
- Angle dependent variation of torque constant k_T .
- Small achievable maximum radial startup distance depending on rotor angle.
- High passive destabilizing radial force and therefore high rotor dynamics.

Angle dependent force variation and x/y coupling are shown in Fig. 6 for our prototype. This effect is characteristic

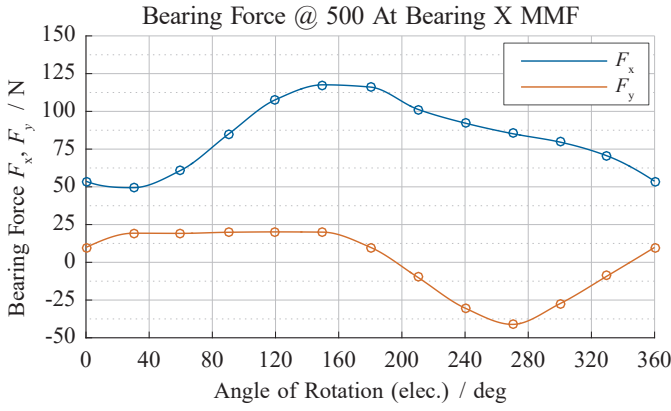


Fig. 6: Angle dependent radial force generation at 500At.

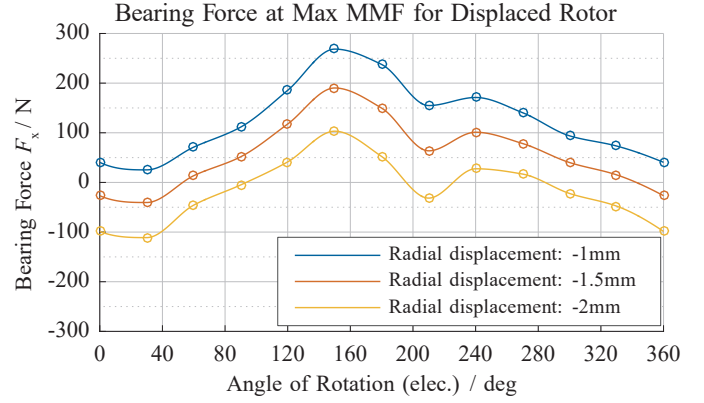


Fig. 9: Angle dependent radial force generation shown for different radial displacements.

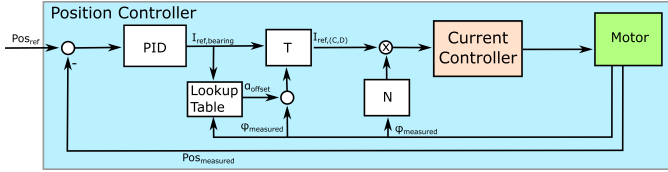


Fig. 7: Used control linearization algorithm to compensate for topology specific angle dependent force fluctuations and angle deviations.

for bearingless reluctance motors, but gets pronounced for decreasing number of stator and rotor teeth. We had to compensate this effect in the control to achieve stable levitation. Fig. 7 shows the implemented control linearization algorithm that was used to operate this machine.

Due to the small teeth number, also angle dependent torque fluctuations are unavoidable (see Fig. 8) and have been documented for mechanical bearing motors [13] and possible compensation strategies were analyzed [14], [15].

Both radial and tangential force components can contribute to bearing forces, while torque is solely generated from tangential forces. FSPM stator teeth are perfect for tangential

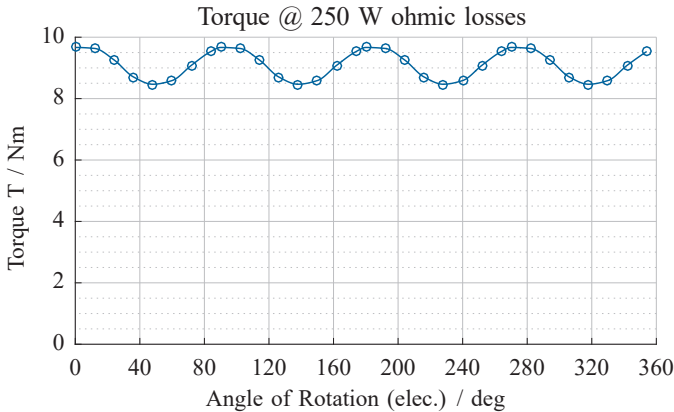


Fig. 8: Angle dependent maximum torque for maximum thermal operating point (250 W ohmic losses).

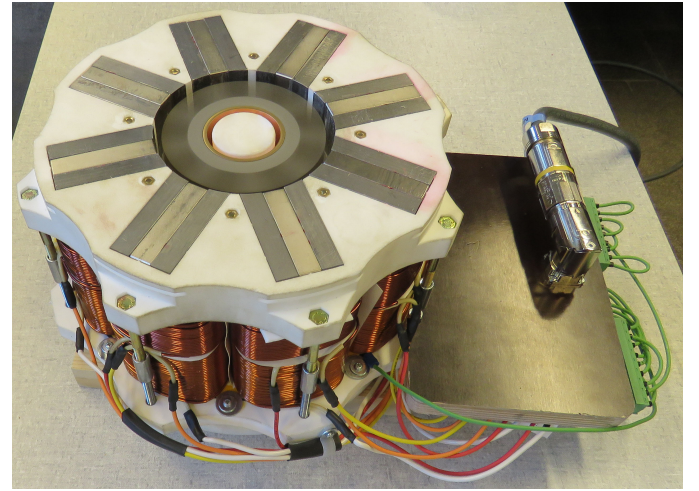


Fig. 10: Running Prototype.

force generation and therefore torque, but no radial force can be generated for example if a rotor tooth is standing in front of the permanent magnet. The radial bearing is therefore relatively weak for bearingless FSPM motors which results in a small maximum radial startup distance, for example 24% of the air gap width in [6]. The angle dependent radial startup characteristic for our prototype is shown in Fig. 9.

The large amount of permanent magnets in the stator, which is used to maximize rotor torque density, does also maximize passive and active radial forces. For our prototype, this has lead to a very high radial rotor dynamic, which needs to be taken care of with a high bandwidth sensor electronics and bearing controller. This is definitely a downside, since sensor noise cannot be properly filtered and is amplified to audible levels.

V. EXPERIMENTAL RESULTS

The prototype was constructed, manufactured, assembled and put into operation (see Fig. 10). A rotational speed of 2000 rpm was reached with stable levitation. At higher rotational speeds radial stability issues can be observed, that are caused

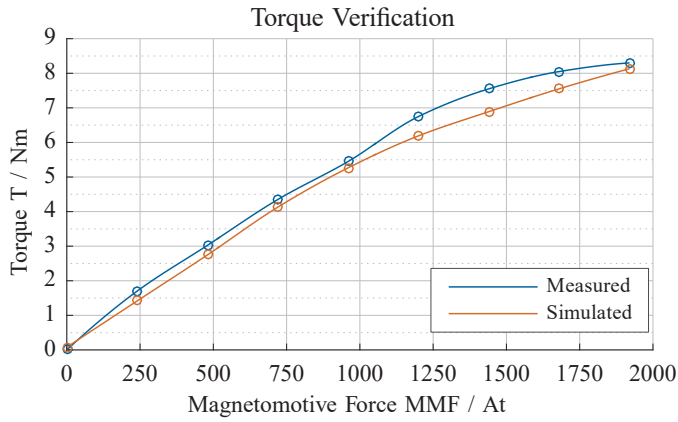


Fig. 11: Torque measurement in standstill and verification of simulation results.

by insufficient bearing force generation bandwidth. This is a result of the destabilizing effect of the massive amount of permanent magnets in the stator, which lead to super fast radial rotor dynamics. The back-EMF voltage limit for this prototype would be located at 4000 rpm.

The passive axial and tilting stiffnesses were measured and match the simulated values quite good. Also the motor torque was validated in standstill. Motor torque versus coil ampere turns is shown in Fig. 11. Without the force linearization algorithm from Fig. 7 stable levitation could not be achieved, even with the rotor not rotating.

Fig. 12 shows bearing and drive currents as well as rotational speed and radial position for a ten second cycle in air for rotational speeds between plus and minus 2000 rpm. The obvious and relatively constant in amplitude fluctuation on the position signal is caused by a small eccentricity on the rotor. This effect is automatically removed in the control algorithm and is therefore not seen in the bearing current.

No-load losses are shown in Fig. 13.

The motor has also been tested with mounted rotor blades in water. The rotor blades with clamp-on mounting mechanism are shown in Fig. 14.

VI. CONCLUSION

The concept and design of a new bearingless slice motor topology providing both higher rotor torque density and larger air gap to rotor diameter ratio compared to previously published topologies has been presented. A 3D FEM optimized prototype was constructed and experimental measurements confirm the simulated performance. This makes the presented motor topology a perfect match for all applications where a steel rotor is beneficial, namely for high circumferential speeds, high ambient temperatures or rotor disposable applications.

ACKNOWLEDGMENT

The authors would like to thank Marcel Schuck for his thorough introduction to paper writing.

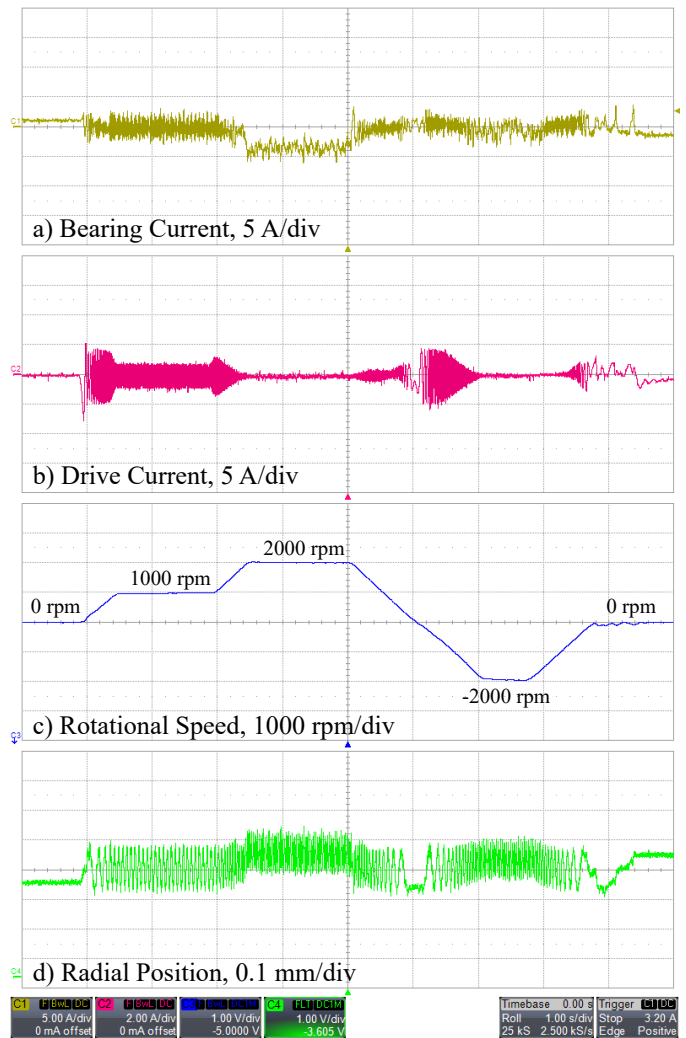


Fig. 12: Measured currents and position for rotational speeds between plus and minus 2000 rpm in air.

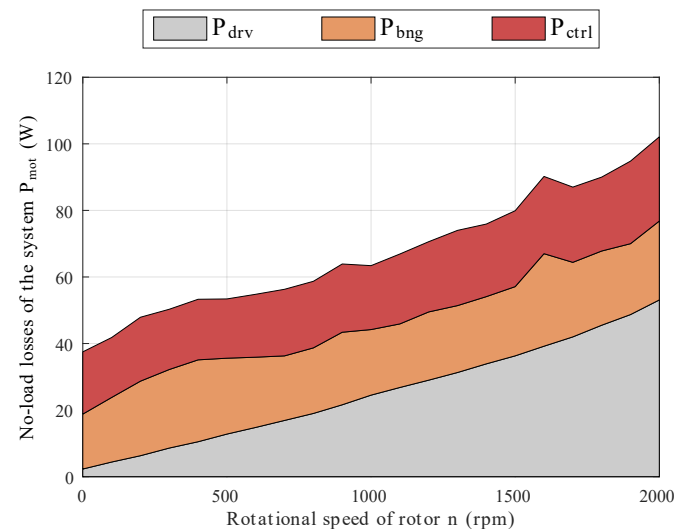


Fig. 13: Measured no-load losses of drive, bearing and power electronics.

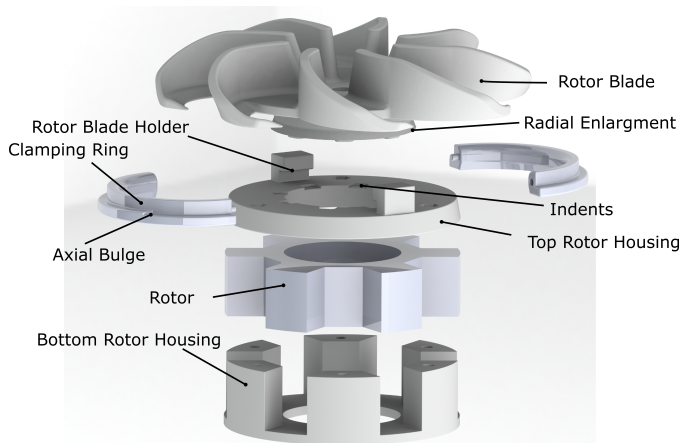


Fig. 14: Rotor with blades and clamp-on mounting mechanism.

- [15] Y. Li, D. Bobba, and B. Sarlioglu, "Design and performance characterization of a novel low-pole dual-stator flux-switching permanent magnet machine for traction application," *IEEE Transactions on Industry Applications*, vol. 52, no. 5, pp. 4304–4314, Sep. 2016.

REFERENCES

- [1] F. De Robertis, E. Birks, P. Rogers, G. Dreyfus, J. Pepper, and A. Khaghani, "Clinical performance with the levitronix centrimag short-term ventricular assist device," *The Journal of heart and lung transplantation*, vol. 25, no. 2, pp. 181–186, 2006.
- [2] R. Schoeb and N. Barletta, "Principle and application of a bearingless slice motor," *JSME International Journal Series C Mechanical Systems, Machine Elements and Manufacturing*, vol. 40, no. 4, pp. 593–598, 1997.
- [3] W. Gruber, W. Briewasser, M. Rothböck, and R. T. Schöb, "Bearingless slice motor concepts without permanent magnets in the rotor," in *Proc. IEEE Int. Conf. Industrial Technology (ICIT)*, Feb. 2013, pp. 259–265.
- [4] W. Gruber, W. Briewasser, and W. Amrhein, "Novel bearingless slice motor design with four concentrated coils featuring a unique operational behavior," in *Proc. 14th European Conf. Power Electronics and Applications*, Aug. 2011, pp. 1–10.
- [5] W. Gruber, M. Rothböck, and R. T. Schöb, "Design of a novel homopolar bearingless slice motor with reluctance rotor," *IEEE Transactions on Industry Applications*, vol. 51, no. 2, pp. 1456–1464, Mar. 2015.
- [6] W. Gruber, K. Radman, and R. T. Schöb, "Design of a bearingless flux-switching slice motor," in *Proc. Int. Power Electronics Conf. (IPEC-Hiroshima 2014 - ECCE ASIA)*, May 2014, pp. 1691–1696.
- [7] Q. Li, P. Boesch, M. Haeffliger, J. W. Kolar, and D. Xu, "Basic characteristics of a 4kW permanent-magnet type bearingless slice motor for centrifugal pump system," in *Proc. Int. Conf. Electrical Machines and Systems*, Oct. 2008, pp. 3037–3042.
- [8] B. Warberger, R. Kaelin, T. Nussbaumer, and J. W. Kolar, "50- /2500-W bearingless motor for high-purity pharmaceutical mixing," *IEEE Transactions on Industrial Electronics*, vol. 59, no. 5, pp. 2236–2247, May 2012.
- [9] F. Zurcher, T. Nussbaumer, W. Gruber, and J. W. Kolar, "Design and development of a 26-pole and 24-Slot bearingless motor," *IEEE Transactions on Magnetics*, vol. 45, no. 10, pp. 4594–4597, Oct. 2009.
- [10] N. Barletta and R. Schoeb, "Design of a bearingless blood pump," *Third International Symposium on Magnetic Suspension Technology*, 1996.
- [11] W. Hua, M. Cheng, Z. Q. Zhu, and D. Howe, "Analysis and optimization of back emf waveform of a flux-switching permanent magnet motor," *IEEE Transactions on Energy Conversion*, vol. 23, no. 3, pp. 727–733, Sep. 2008.
- [12] J. T. Chen and Z. Q. Zhu, "Comparison of all- and alternate-poles-wound flux-switching pm machines having different stator and rotor pole numbers," *IEEE Transactions on Industry Applications*, vol. 46, no. 4, pp. 1406–1415, Jul. 2010.
- [13] A. Lindner and I. Hahn, "Design of an e-core flux-switching permanent magnet machine with large air-gap," in *Proc. IEEE Int. Electric Machines Drives Conf. (IEMDC)*, May 2015, pp. 1580–1585.
- [14] A. Lindner, H. Kurtović, and I. Hahn, "Investigation of parametrized curves for the pole shaping in an e-core flux-switching machine with large air-gap," in *Proc. 8th IET Int. Conf. Power Electronics Machines and Drives (PEMD 2016)*, Apr. 2016, pp. 1–5.